# SWITCHABLE SPLIT-RING FREQUENCY SELECTIVE SURFACES

**M. H. B. Ucar, A. Sondas, and Y. E. Erdemli**

Electronics and Computer Education Department
Kocaeli University, Umuttepe
Kocaeli 41380, Turkey

**Abstract**—Tunable frequency selective surfaces (FSSs) based on split ring resonators (SRRs) are presented. Tuning performance is achieved by means of several on/off switches placed between the rings of each SRR element. The band-stop FSS response is dynamically tuned to different frequency bands at different switching states. In addition, loadings placed at the corners of outer ring elements, forming a fan-like shape, with additional switches are shown to offer rather fine-tuning capability. A dual-layer FSS is also introduced to demonstrate a filter response over a larger frequency band, and also offers tunable dual-band operation via switching. By using complementary SRR elements, a tunable band-pass response instead can be obtained using a similar switching configuration. Practical switch modeling is also examined in the paper along with the scanning performance of the SRR-FSS. The numerical analysis of the FSS designs is accomplished using a fast periodic array simulator, and the measurements demonstrate preliminary validation of the proposed switching configuration.

## 1. INTRODUCTION

There has been a significant interest in frequency selective surfaces (FSSs) since early 1960s. A large body of knowledge and design techniques exists for FSSs which have been utilized as electromagnetic filters in a variety of wireless communication applications [1]. An FSS is basically a periodic array of metallic elements or apertures backed by a dielectric slab, and these FSS elements can be realized as different geometrical shapes (e.g., patch, loop, cross, split-ring, etc.). FSSs exhibit exceptional reflection/transmission characteristics over a frequency band of interest which is determined by the resonance behavior of the corresponding element. The FSS design and fabrication

is entirely based on printed circuit technology, which makes the construction rather easy. Moreover, multiple layers of FSS can increase design flexibility. In this context, multilayer FSS configurations can be employed for use in broad-band or multi-band applications [1–3].

In this paper, we introduce novel FSS designs based on split ring resonator (SRR) elements. SRR arrays were initially proposed as metamaterial structures demonstrating $\mu$-negative behavior, yielding band-stop response in a specific frequency band [4]. Recently, SRRs have been employed as FSS elements to provide a similar filter response [5, 6]. Here we consider frequency-tunable FSSs based on SRR elements. Frequency-tuning performance is achieved by means of on/off switches placed between the rings of each SRR element. This switching configuration was originally introduced for a composite left-handed slab whose band-pass response could be dynamically tuned to different frequency bands [7]. A similar switching was also successfully employed in a SRR-based microstrip filter design, providing tunable single-band or dual-band frequency responses [8]. In addition, loadings placed at the corners of outer ring elements, forming a fan-like shape (fan SRR: FSRR), with additional switches is shown to allow for rather fine-tuning operation. A dual-layer SRR (DSRR) arrangement is also presented to demonstrate a filter response over a larger frequency range, and also offers tunable dual-band performance by means of switching. Complementary-SRR (CSRR) elements are as well considered to achieve a tunable band-pass response using a similar switching configuration.

In the paper, we present simulation results to demonstrate multi-frequency performance of the proposed FSS designs, namely, SRR-FSS, FSRR-FSS, DSRR-FSS, and CSRR-FSS. We note that the numerical analysis of the designs is achieved by means of a well-validated periodic array simulator [2, 3, 9]. We also present measured data for SRR-FSS prototypes as a preliminary validation for the proposed switching configuration. While the switches are initially modeled as metallic pads placed between the rings at appropriate locations, simplistic PIN diode and micro-electro-mechanical-system (MEMS) switch models are incorporated into the SRR-FSS design to demonstrate practical switch performance.

## 2. SWITCHABLE FSS DESIGNS

The numerical analysis of the FSS designs was carried out by means of a periodic array simulator based on the hybrid finite element-boundary integral (FE-BI) method in conjunction with the fast spectral domain algorithm (FSDA) [9]. In the simulator is only one unit cell of

the periodic array modeled and the structure is presumed to be infinite-periodic in the $x$-$y$ plane and finite-periodic in the $z$-dimension. Below we present the transmission characteristics of the proposed FSS designs, namely SRR-FSS, FSRR-FSS, DSRR-FSS, and CSRR-FSS.

## 2.1. SRR-FSS

The unit cell configuration of the SRR-FSS design is shown in Fig. 1. The ring resonators are modeled using zero-thickness metallic elements which are supported by a substrate of $\varepsilon_r = 3.0$ with thickness $h = 0.6$ mm. The on/off switches ($S_1$, $S_2$, $S_3$) are modeled as metallic pads ($0.3 \times 0.3$ mm$^2$) placed along the rings at optimized locations. This switching configuration is similar to the one in [7]. We note that the presence of a metallic pad in a switch location refers to the switch being in on-state, otherwise, in off-state.
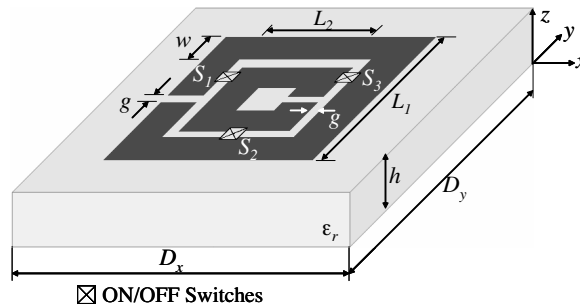


**Figure 1.** Unit cell configuration of the SRR-FSS: $L_1 = 5.7$, $L_2 = 3.3$, $g = 0.3$, $w = 0.9$, $h = 0.6$, $D_x = D_y = 7.5$ (all in mm), $\varepsilon_r = 3$.

The frequency response of the SRR-FSS is displayed in Fig. 2. As seen, the band-stop response occurs around 5.4 GHz when all of the switches are in off-state (opened). By turning on (closing) each switch at a time, the band-stop response can be tuned to respective frequencies. As seen in Fig. 2, the switch placed equidistant from each of the splits ($S_2$) provides for operation around 4.25 GHz whereas the switch closer to the split of the outer ring ($S_1$) and the switch closer to the split of the inner ring ($S_3$) allow for operation at a lower band (around 3.85 GHz) and at a higher band (around 4.6 GHz), respectively. Hence, the tunable SRR-FSS offers multi-frequency band-stop response over 3.8–5.5 GHz band. In addition, by varying the locations of the switches around the loop between the rings, the corresponding resonant frequencies ($f_r$) can be adjusted to desired frequencies as shown in Fig. 3.
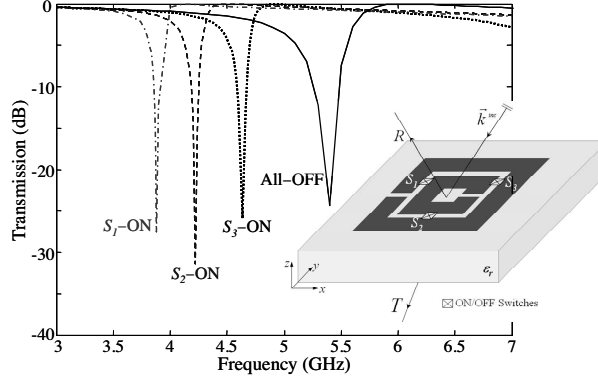
**Figure 2.** Frequency-tuning performance of the SRR-FSS at normal incidence (TE-pol, $\theta = \phi = 0°$).

We also examined scanning performance of the SRR-FSS. The related data for TE polarized (TE-pol) incident waves are displayed in Fig. 4. As seen, the band-stop FSS behavior is fairly well maintained for different incidence angles. However, an increase in bandwidth is observed for oblique incidences due to more pronounced magnetic resonance characteristic. On the other hand, for TM polarized (TM-pol) waves, the band-stop response was observed to vanish towards the horizon. In addition, the computed cross-polarization levels were below $-20\,\text{dB}$ and $-8\,\text{dB}$ for the TE-pol and TM-pol cases, respectively, for oblique incidences. This polarization sensitivity, in fact, is expected due to non-symmetrical geometry of the FSS element.

## 2.2. FSRR-FSS

As discussed above, the switchable SRR-FSS provides tunable operation with four different bands where each band is apart about $0.5\,\text{GHz}$. In order to offer rather fine-tuning capability, we included metallic loadings at the corners of outer ring elements, forming a fan-like shape (fan SRR: FSRR), and placed additional switches (namely, $S_4$ and $S_5$) along those extensions. The unit cell configuration of the FSRR-FSS design along with the corresponding frequency response is shown in Fig. 5. As seen, while the switches inserted between the rings ($S_1/S_2/S_3$) provide coarse tuning ($\sim 0.5\,\text{GHz}$) operation, the switches placed along the loadings ($S_4/S_5$) yield rather fine frequency-tuning ($\sim 0.1\,\text{GHz}$) performance. Thus, the designer would have degrees of freedom while choosing appropriate switch configuration depending on operational frequency of application at hand.
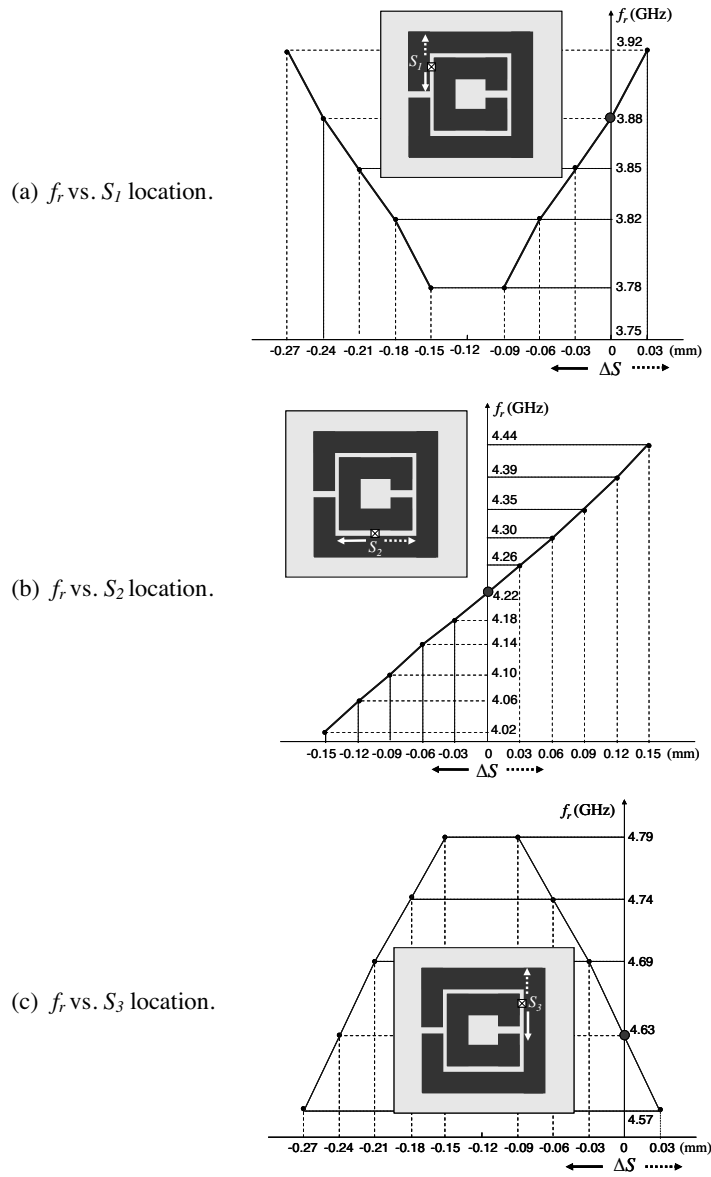
(a) $f_r$ vs. $S_1$ location.



(b) $f_r$ vs. $S_2$ location.



(c) $f_r$ vs. $S_3$ location.

**Figure 3.** Tuning the resonance frequency ($f_r$) of the SRR-FSS design by varying the switch locations. $\Delta S$ represents the distance from the designated switch locations.
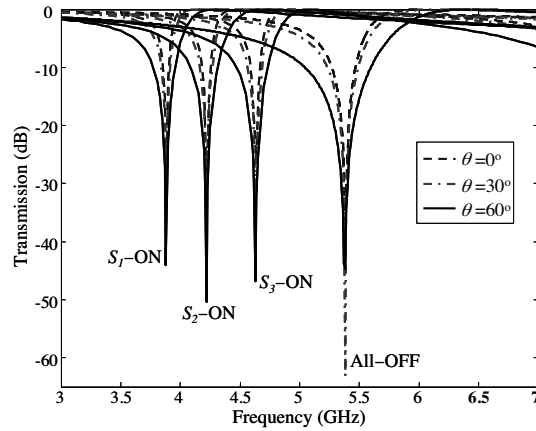
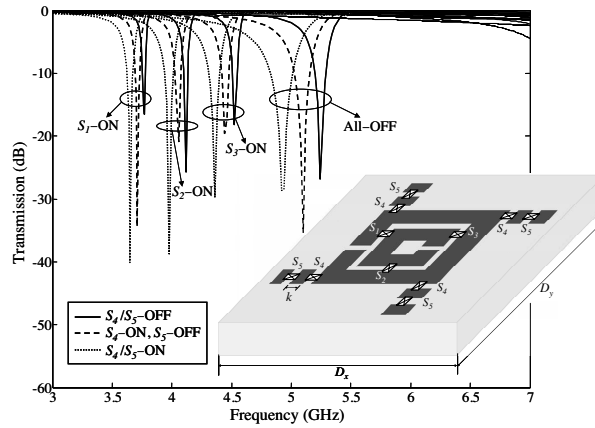**Figure 4.** Scanning performance of the tunable SRR-FSS design (TE-pol, $\phi = 0°$).



**Figure 5.** Frequency-tuning performance of the FSRR-FSS at normal incidence (TE-pol, $\theta = \phi = 0°$). $D_x = D_y = 9.9$ mm and $k = 0.6$ mm; all other parameters are same as those of the SRR-FSS design (see Fig. 1).

## 2.3. DSRR-FSS

Multilayer FSS structures can be constructed by simply cascading several FSS layers. The goal of multilayer configuration here is to broaden the frequency response of the FSS. Such a dual-layer FSS design and the corresponding transmission characteristics are shown

in Fig. 6. Each layer (Layer-1/Layer-2) was designed individually to provide a band-stop response at 4.6 GHz and 5.4 GHz, respectively. In fact, the layer designated as Layer-1 is same as the SRR-FSS design (see Fig. 1) in absence of switches. The unit cell $(D_x, D_y)$ and ring dimensions of Layer-2 $(w, L_1, L_2)$ were chosen to be almost 1.25 times those of Layer-1. Since the layers now have different periodicities, the dual-layer configuration is referred to as non-commensurate and such a structure is analyzed via the periodic array simulator in an approximate manner [2]. By placing these layers in cascade, we optimized the distance between the layers to achieve a wider rejection band centered around 5.2 GHz as seen in Fig. 6. Furthermore, we considered a switched DSRR-FSS configuration, yielding a tunable dual-band filter response as displayed in Fig. 7. As shown, for each layer, there is one switch $(S_{1,i}, i = 1, 2)$ placed between the rings nearby each outer split. When the switch on Layer-1 $(S_{1,1})$ is closed with the switch on Layer-2 $(S_{1,2})$ opened, the DSRR-FSS results in a dual-band rejection response around 3.8 GHz and 5.15 GHz. When the switch positions are reversed, the dual-band response shifts to about 3.65 GHz and 5.3 GHz, respectively; that is, the rejection bands are further separated.
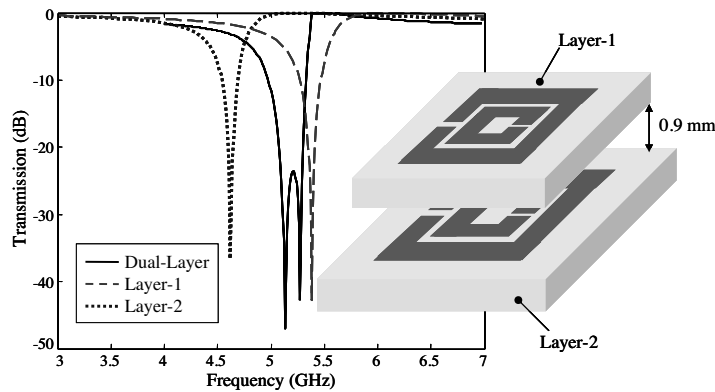


**Figure 6.** Transmission characteristics of the DSRR-FSS at normal incidence (TE-pol, $\theta = \phi = 0°$).

## 2.4. CSRR-FSS

Referring to Babinet's principle, by using a complementary SRR configuration instead, a band-pass FSS response can be obtained. Such an FSS design with a similar switching configuration is depicted in
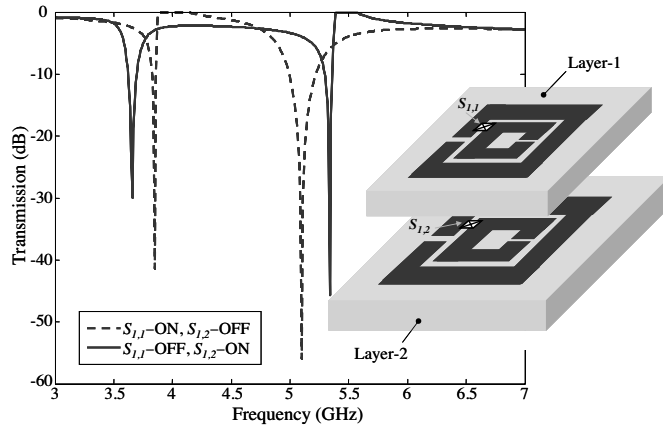
**Figure 7.** Transmission characteristics of the tunable DSRR-FSS at normal incidence (TE-pol, $\theta = \phi = 0°$).



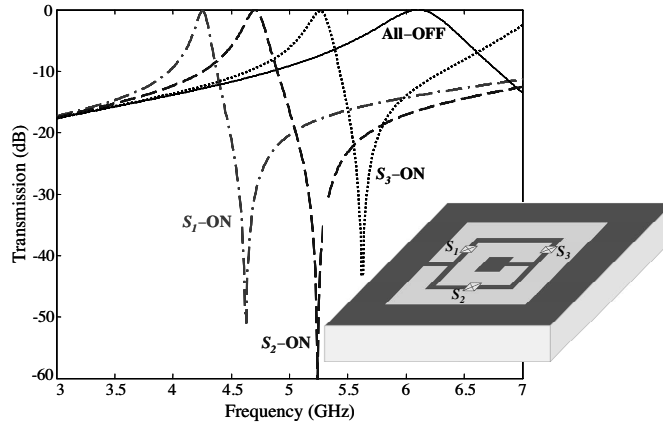**Figure 8.** Frequency-tuning performance of the switchable CSRR-FSS at normal incidence (TM-pol, $\theta = \phi = 0°$).

Fig. 8 along with the corresponding filter response. We note that all of the dimensions for the CSRR-FSS unit cell were kept the same as those of the SRR-FSS geometry (see Fig. 1). However, in this case, the presence of a metallic pad in a switch location refers to the switch being in off-state, otherwise, in on-state. As seen in Fig. 8, a rather larger transmission band occurs around 6.1 GHz when all of the switches are in off-state. By turning on each switch at a time, the band-pass response can be tuned to respective frequencies. As shown, the

switches $S_1$, $S_2$, and $S_3$ allow for operation around 4.25 GHz, 4.7 GHz, and 5.25 GHz, respectively. Thus, the tunable CSRR-FSS offers multi-frequency band-pass response over 4.0–6.5 GHz band. We remark that while the SRR-FSS offers a band-stop response for the TE-pol case, the CSRR-FSS provides a band-pass response for the TM-pol case, an expected behavior of such complementary structures.

## 3. MEASUREMENTS

In order to validate the proposed switching configuration for the SRR-FSS design (see Fig. 1), two FSS panels were fabricated and free-space transmission measurements were carried out. One of the panels consists of SRR elements with no metallic pads, referring to all switches being in off-state, while the other one includes pads in $S_3$ switch locations only (that is, $S_3$-ON and $S_1/S_2$-OFF) as displayed in Fig. 9. Each panel consists of $37 \times 30$ metallic SRR elements (overall size: $27.8 \times 22.8$ cm$^2$) etched on an RO3003 substrate with dielectric constant of $\varepsilon_r = 3.0 \pm 0.04$ ($\tan \delta = 0.0013$) and thickness $h = 0.0508$ cm (0.02 inch). The corresponding measurements were carried out using the setup comprised of two standard-gain horn antennas (1–18 GHz, ETS-Lindgren Model-3115) and Agilent$^{\text{TM}}$ E8362B PNA network analyzer as shown in Fig. 10. The measured and related simulated data are displayed in Fig. 11. As seen, the responses of the finite-size FSS panels are predicted fairly well by the simulated infinite-size SRR-FSS designs with a slight downward frequency-shift of about 0.25 GHz. More importantly, the frequency-tuning performance is demonstrated with this preliminary realization.
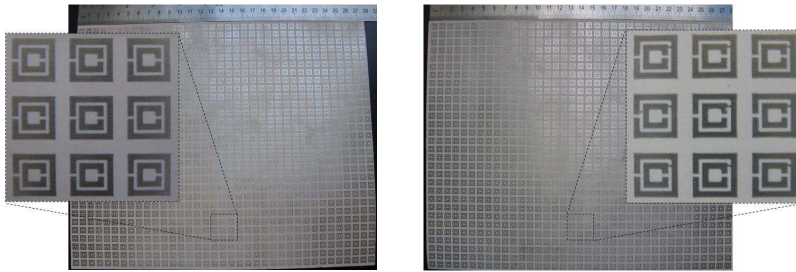


**Figure 9.** Fabricated SRR-FSS panels without (left) and with (right) metallic pads (in $S_3$ switch locations).

It is important to point out that the simulated data shown in Fig. 11 are not the replica of those displayed in Fig. 2 where the SRR-FSS design with the parameters given in Fig. 1 is considered. In fact,
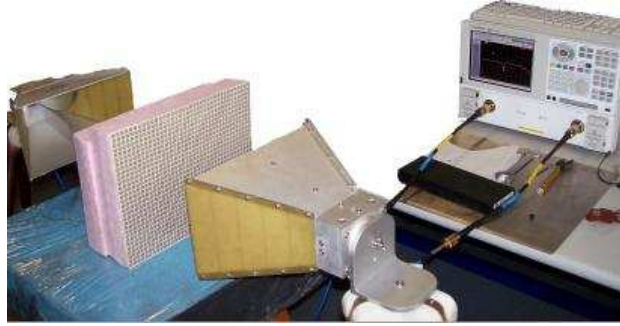
**Figure 10.** Setup used for transmission measurements of the SRR-FSS panels.
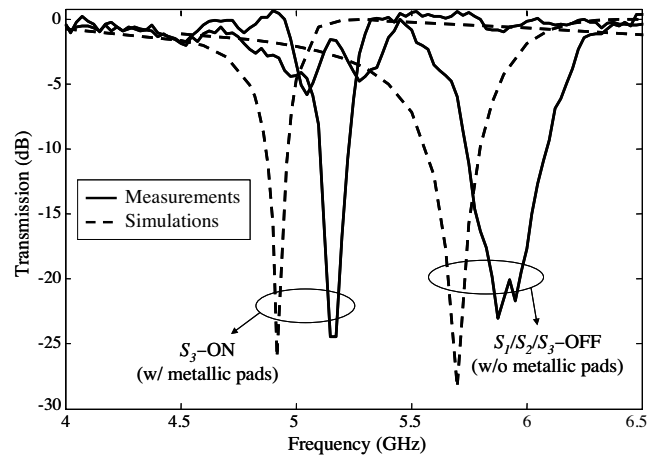


**Figure 11.** Simulated and measured transmission responses of the SRR-FSS designs.

the previous simulated FSS responses (Fig. 2) have about 0.25 GHz lower resonant frequencies as compared to the current simulation results (Fig. 11). There are several reasons for those differences. The substrate thickness $h$ originally was 0.06 cm, but the fabricated panels had $h$=0.0508 cm, with which the SRR-FSS was then re-modeled. Also, while re-meshing the structure in the simulator, two prism layers were used instead of just one for a more accurate modeling of the substrate. Those two changes applied in the simulations were shown to contribute almost 0.2 GHz upward frequency shifts in the corresponding FSS responses. Moreover, when the realized

metallic thicknesses of $35\,\mu\text{m}$ along with the designated tolerance values for $\varepsilon_r$ were considered in the re-modeling, an additional $0.05\,\text{GHz}$ upward frequency-shift was achieved in the responses, thus resulting in optimum agreement between the measured and predicted data as seen in Fig. 11. We also note that more sensitive far-field measurements with larger FSS panels would yield better agreement with the simulations.

## 4. ACTUAL SWITCH MODELING

For practical implementation of the switchable SRR-FSS designs, surface-mounted PIN diode or MEMS switches would be the preferred choice due to their compact, low-loss and high-isolation features [10, 11]. To demonstrate possible effects of practical switches on the FSS performance, we included simple equivalent models for the switches (in lieu of metallic pads) in the analysis and the corresponding simulations carried out as discussed below.

### 4.1. Pin Diode Modeling

In PIN diode modeling, the switches were modeled as capacitors ($C = 0.3 - 1\,\text{pF}$) and resistors ($R = 1\,\Omega$) when they are in off-state and in on-state, respectively, as displayed in Fig. 12. Those capacitor and resistor values represent actual switch behavior in an approximate manner. A representative FSS performance with the switch model is shown in Fig. 13. As seen, by the inclusion of the switch model, there is almost no effect observed in the response when all switches are in off-state. However, the frequency response is shifted downward slightly ($\sim 0.1\,\text{GHz}$) and the corresponding suppression levels increase somewhat for the case only $S_3$ switch in on-state as compared to the response of the metallic-pad modeling. These differences, in fact, are expected and demonstrate tolerable switch effects in a practical implementation.

### 4.2. MEMS Switch Modeling

In MEMS switch modeling, the switches were modeled as two-legged bridges based on cantilever MEMS switch structure [12] as depicted in Fig. 14. As seen, this simplistic model consists of a resistive card ($R_c\,\Omega/\text{cm}^2$) placed on two metal legs where $R_c$ represents possible losses when the switch is in on-state. As for the off-state, there is no loss definition specified for one-legged structure, while a possible capacitive effect is expected. The transmission characteristics for the SRR-FSS
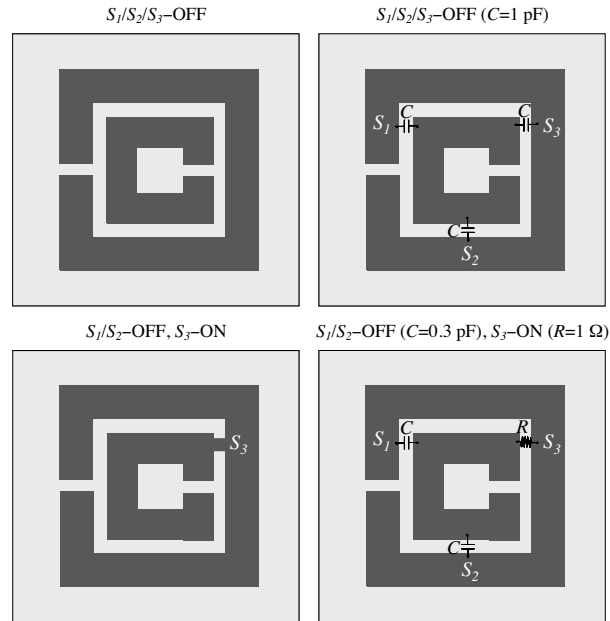
**Figure 12.** Metallic-pad modeling (left column) and equivalent PIN-diode modeling (right column) of the switches in the SRR-FSS design.
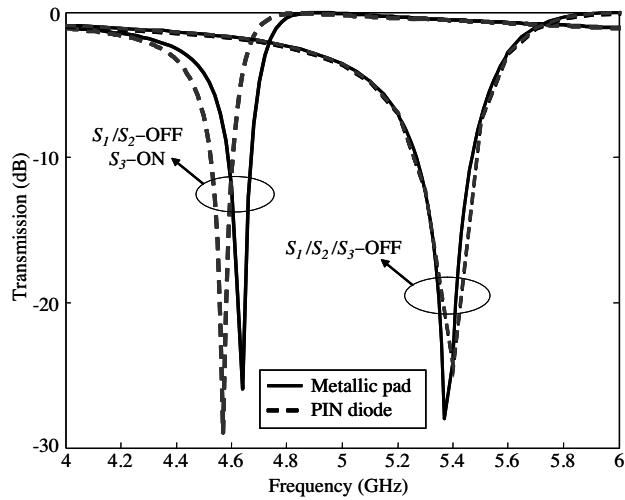


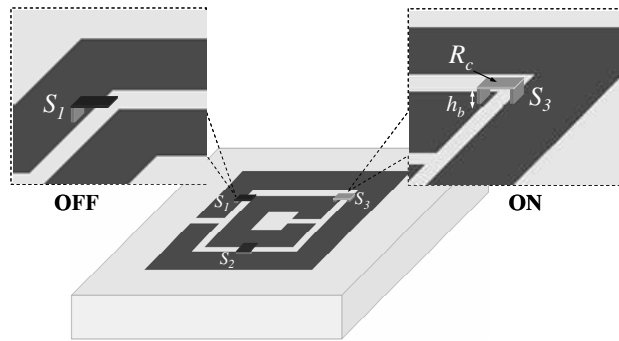**Figure 13.** Effects of PIN-diode equivalent circuit modeling on the FSS performance.

**Figure 14.** MEMS switch modeling in the SRR-FSS design (the modeling for $S_1/S_2$-OFF, $S_3$-ON is shown).
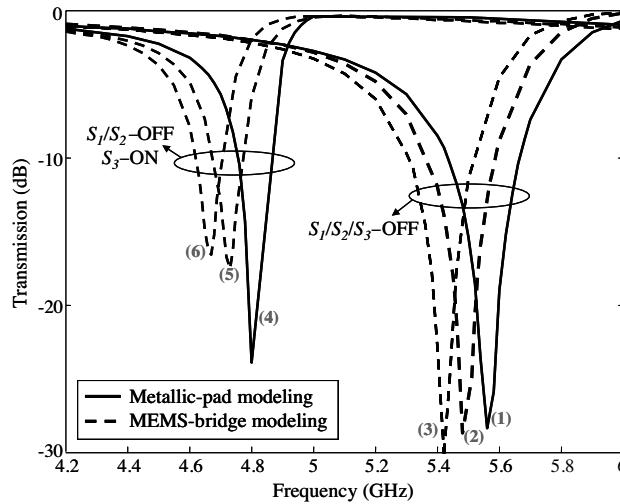


**Figure 15.** Effects of MEMS-bridge modeling on the SRR-FSS performance. Simulations for metallic-pad modeling (1 & 4) and MEMS modeling (see Fig. 14) for (2) $h_b = 0.1$ mm, (3) $h_b = 0.05$ mm, (5) $h_b = 0.1$ mm, $R_c = 1\,\Omega$ and (6) $h_b = 0.05$ mm, $R_c = 0.5\,\Omega$ are displayed.

designs with MEMS switch models are displayed in Fig. 15. As seen, by the inclusion of the switch model, the responses are shifted downward slightly (0.05–0.1 GHz) for both switching states (i.e., all in off-state and only $S_3$ on-state) due to expected capacitive loading imposed by the bridge structure as compared to those of the metallic-pad modeling.

In addition, the corresponding suppression levels decrease almost 6 dB for the latter switching state due to loss introduced by the resistive cards. In brief, MEMS switch modeling demonstrates acceptable switch performance in an actual implementation.

## 5. CONCLUSION

In the paper, tunable FSS designs using SRR elements along with on/off switches have been introduced. The corresponding simulations supported by measurements demonstrated that the band-stop filter response for the switchable SRR-FSS design could be dynamically tuned to different frequency bands over the frequency band of interest. In addition, it was shown numerically that the use of actual switches would have a minimal effect on the FSS performance. Polarization and incidence angle sensitivity of the SRR-FSS were also examined. In addition, switchable fan-like FSRR-FSS design was shown to provide rather fine-tuning capability. The SRR-FSS design was extended to include multiple FSS layers (namely, DSRR-FSS), offering larger bandwidth and dual-band performance via switching. The complementary version of the design (CSRR-FSS) was also presented, providing tunable band-pass filter response. To conclude, novel switchable FSS designs are proposed in the paper with noting that implementation difficulties, such as mounting and biasing of the switches, should be assessed in realization.

## ACKNOWLEDGMENT

## REFERENCES

1. Munk, B. A., *Frequency Selective Surfaces: Theory and Design*, John Wiley & Sons, New York, 2000.
2. Erdemli, Y. E., K. Sertel, R. A. Gilbert, D. E. Wright, and J. L. Volakis, "Frequency-selective surfaces to enhance performance of broad-band reconfigurable arrays," *IEEE Trans. Antennas Propagat.*, Vol. 50, No. 12, 1716–1724, 2002.
3. Erdemli, Y. E., R. A. Gilbert, and J. L. Volakis, "A reconfigurable slot aperture design over a broadband substrate/feed structure,"

*IEEE Trans. Antennas Propagat.*, Vol. 52, No. 11, 2860–2870, 2004.

4.  Pendry, J. B., A. J. Holden, D. J. Robins, and W. J. Stewart, "Magnetism from conductors and enhanced nonlinear phenomena," *IEEE Trans. Microwave Theory Tech.*, Vol. 47, No. 11, 2075–2084, 1999.

5.  Beruete, M., R. Marques, J. D. Baena, and M. Sorolla, "Resonance and cross-polarization effects in conventional and complementary split ring resonators periodic screens," *Proc. IEEE Antennas Propagat. Soc. Int. Symp.*, 794–797, Washington D.C., July 3–8, 2005.

6.  Bardi, I., R. Remski, D. Perry, and Z. Cendes, "Plane wave scattering from frequency-selective surfaces by the finite-element method," *IEEE Trans. Magnetics*, Vol. 38, No. 2, 641–644, 2002.

7.  Erdemli, Y. E. and A. Sondas, "Dual-polarized frequency-tunable composite left-handed slab," *Journal of Electromagnetic Waves and Applications*, Vol. 19, No. 14, 1907–1918, 2005.

8.  Cenk, C., A. Sondas, and Y. E. Erdemli, "Tunable split ring resonator microstrip filter design," *Proc. Mediterranean Microwave Symposium*, 20–23, Genova, Italy, Sep. 19–21, 2006.

9.  Eibert, T. F., Y. E. Erdemli, and J. L. Volakis, "Hybrid finite element-fast spectral domain multilayer boundary integral modeling of doubly periodic structures," *IEEE Trans. Antennas Propagat.*, Vol. 51, No. 9, 2517–2520, 2003.

10.  Chang, T. K., R. J. Langley, and E. A.Parker, "Active frequency-selective surfaces," *IEE Proc-Microw. Antennas Propag.*, Vol. 143, No. 1, 62–66, 1996.

11.  Schoenlineer, B., A. Abbaspour-Tamijani, L. C. Kempel, and G. M. Rebeiz, "Switchable low-loss RF MEMS Ka-band frequency-selective surface," *IEEE Trans. Microwave Theory Tech.*, Vol. 52, No. 11, 2474–2481, 2004.

12.  Rebeiz, G. M. and J. B. Muldavin, "RF-MEMS switches and switch circuits," *IEEE Microwave Magazine*, Vol. 2, No. 4, 59–71, 2001.